Applied Catalysis B: Environmental 258 (2019) 117967

Contents lists available at ScienceDirect

Applied Catalysis B: Environmental

journal homepage: www.elsevier.com/locate/apcatb

The pulsed laser-induced Schottky junction via in-situ forming Cd clusters on CdS surfaces toward efficient visible light-driven photocatalytic hydrogen evolution

Wenwu Zhong[a,*,1], Shijie Shen[a,1], Min He[b], Da Wang[c], Zongpeng Wang[a], Zhiping Lin[a], Wenguang Tu[d,*], Jiaguo Yu[e,*]

[a] Department of Materials, Taizhou University, Taizhou, 318000, China
[b] School of Opto-Electric Information Science and Technology, Yantai University, Yantai, 264005, China
[c] Research & Development Center for Functional Crystals, Beijing National Laboratory for Condensed Matter Physics, Institute of Physics, Chinese Academy of Sciences, Beijing 100190, China
[d] School of Mechanical & Aerospace Engineering, Nanyang Technological University, Singapore, 637459, Singapore
[e] State Key Laboratory of Advanced Technology for Materials Synthesis and Processing, Wuhan University of Technology, Wuhan 430070, PR China

ARTICLE INFO

Keywords:
CdS
Pulsed laser treatment
Metal Cd clusters
Photocatalytic hydrogen production
Schottky junction

ABSTRACT

Herein, we developed one simple and novel post-treatment technique via pulsed laser irradiation of CdS (L-CdS) semiconductor to significantly enhance the visible light-driven hydrogen evolution performance from water splitting, during which the rate of hydrogen evolution over L-CdS in the first hour is 40-times than that of pure CdS. Because the pulsed laser irradiation induces the in-situ formation of metallic Cd clusters on CdS surface to construct the Schottky junction between Cd clusters and CdS, obviously facilitating the electron transfer from excited CdS into Cd to endow more photogenerated electrons for enhancing the photocatalytic efficiency of H_2 evolution. Moreover, the bandgap narrow of post-treated CdS also benefits the stronger light absorption for enhancing the photocatalytic efficiency. This work may provide a new approach to develop heterojunction-based photocatalysts for efficient solar-to-chemical conversion.

1. Introduction

In recent decades, researches on finding energy sources have received increasing attentions as global energy demand continues to grow [1–3]. Hydrogen energy has been widely regarded as an ideal non-polluting green energy source, due to its advantages such as high efficiency, storability, and transportation [4–8]. In 1972, Fujishima and Honda [9] first reported the phenomenon that photocatalytic decomposition of water by TiO_2 single crystal electrode to generate hydrogen, thus revealing the possibility of water splitting into hydrogen driven by solar energy. Subsequently, a large amount of ultraviolet light-responsive metal oxide photocatalysts are researched for solar-driven H_2 evolution from water splitting, mainly including transition metal oxides with d^0 electronic structure (such as ZrO_2, Nb_2O_5, and Ta_2O_5 et al) [10–12] and metal oxides with d^{10} configuration (such as Ga_2O_3, In_2O_3, and SnO_2 et al) [13–16]. However, only 3%–4% of the solar spectrum absorbed by these metal oxide photocatalysts limits their efficiency.

In order to extend the light-harvesting range, numerous visible light-responsive photocatalysts such as WO_3, $BiVO_4$, and Fe_2O_3 et al. [17,18] are also explored. Among these visible light-responded photocatalysts, CdS is one of promising semiconductors for photocatalytic hydrogen evolution, because its narrow bandgap of 2.4 eV allows it to effectively make use of solar light below 520 nm [19–23]. Compared to the metal oxide photocatalysts, the more negative conduction band potential of CdS also makes it to be more suitable for water splitting into hydrogen [24,25]. Unfortunately, the hydrogen production efficiency over CdS is still relatively low due to the fast recombination rate of photogenerated charge carriers [26].

A lot of strategies are employed to reduce the recombination rate of charge carriers. One of the widely used methods is morphology control that exploring various morphologies of CdS from 0-dimensional to 1-dimensional and 2-dimensional nanostructures [27–35]. With the surface volume ratio increases, the shortening of path of carrier transport could reduce the recombination rate. In addition, the development of

* Corresponding authors.
E-mail addresses: zhongww@tzc.edu.cn (W. Zhong), wgtu@ntu.edu.sg (W. Tu), jiaguoyu@yahoo.com (J. Yu).
[1] These authors contributed equally to this work.

https://doi.org/10.1016/j.apcatb.2019.117967
Received 9 June 2019; Received in revised form 11 July 2019; Accepted 15 July 2019
Available online 24 July 2019
0926-3373/

surface/interface heterojunction between CdS and co-catalysts is also one of potential solutions to enhance interfacial charge carrier separation and transfer [36]. Up to now, various co-catalysts (such as Pt [37], Ni [38], Ni_2O_3 [39], Ni_2P [40], NiS_2 [41], $Co(OH)_2$ [42], CoO_x [43], MoS_2 [44], MoP [45], $Cd(OH)_2$ [46], Cd [47,48], graphene [49–51], et al.) have been explored to enhance photocatalytic hydrogen production efficiency of CdS. However, the insufficient contact between CdS and these co-catalysts also restricts the charge carrier transfer and the enhancement of photocatalytic activity.

Here, we construct one CdS/Cd Schottky junction photocatalyst using the novel and ultrafast pulsed laser technique to improve visible light-driven hydrogen evolution from water splitting, during which the laser bombardment could destroy Cd-S bonds on CdS surface to form metallic Cd clusters on CdS surface. The 40-times enhancement of photocatalytic activity of CdS/Cd in first hour compared to pure CdS results from: 1) metallic Cd clusters serve as electron sinks to accept the excited electrons from CdS via Schottky junction to minimize electron-hole recombination; 2) the post-treated CdS shows stronger adsorption capacity of the sacrificial agents such as S^{2-} and SO_3^{2-} to promote the consumption of photogenerated holes; 3) the bandgap narrow of post-treated CdS also benefits the stronger light absorption. This work may provide a new approach to develop heterojunction-based photocatalysts for efficient solar-to-chemical conversion.

2. Experimental

2.1. Preparation of CdS photocatalyst

The preparation of CdS photocatalyst was similar with the previous work [25]. An equimolar ratio of $Cd(CH_3CO_2)_2$ (99.99%) was mixed with an aqueous solution of Na_2S (99.99%). After the mixing solution was stirred for 24 h, the resulting yellow precipitate was collected. Then, the precipitate was dispersed in 72 mL of deionized water and sealed in a reaction kettle for 72 h at 200 °C. The precipitate was washed twice with alcohol and then dried for 24 h to obtain the yellow CdS powder.

2.2. Pulsed laser treatment of CdS photocatalyst

The laser irradiation of CdS sample was performed using a Nd:YAG pulsed laser with the wavelength of 1064 nm (Continuum PRII-8000) [52]. The CdS powder was uniformly coated on a silica glass substrate with the size of 1 cm × 1 cm, which was vertically illuminated by a pulsed laser (the pulse duration is 8 ns and the frequency is 10 Hz) with scan mode in 1 W. The total duration of light irradiation is 1 min. The laser irradiated sample was named L-CdS.

2.3. Characterization

The X-ray powder diffraction (XRD) characterization was conducted on a Philips X'pert Pro diffractometer with radiation wavelength of 1.54 Å. The annular-bright-field (ABF) imaging was measured on a scanning transmission electron microscope (STEM) coupled with a spherical aberration corrector. The SEM was characterized on a S-4800. The fourier transform infrared (FT-IR) spectra were characterized by a Nicolet-6700 spectrometer. The X-ray photoelectron spectroscopy was characterized on a ESCALAB Mk II spectrometer with Al Kα X-rays, and the binding energy was corrected by the C1s signal. The UV–vis diffuse reflection spectra were obtained by an instrument UV-2550 (Shimadzu) using $BaSO_4$ as the reflection standard. The electron paramagnetic resonance (EPR) measurements were performed using a Bruker Elexsys E-500 spectrometer at room temperature. The setting parameters of EPR are as following: modulation frequency: 100.00 KHz, modulation amplitude: 2.00 G, sweep width: 100.00 G, time constant: 40.960 ms, conversion: 40.000 ms, sweep time: 80.720 s.

2.4. Photocatalytic experiment

Photocatalytic water splitting into hydrogen was carried out in one Labsolar II system (Beijing perfectlight technology co. LTD). 20 mg of the photocatalyst was placed in 100 mL of solution containing 0.1 mol/L of Na_2S and Na_2SO_3 as sacrificial agents. The light source is 300 W Xe lamp via the filter with cut-off wavelength of 420 nm. Before irradiation, the system was vacuumed for 10 min via the vacuum pump to completely remove the dissolved oxygen. The generated gas was analysed by the gas chromatograph (GC7890II, Techcomp) using nitrogen gas as a carrier gas and a molecular sieve with a pore diameter of 5 Å. The stability performed in condition that the photocatalyst was used, re-collected and re-used for multiple times. The apparent quantum efficiency (QE) was measured under the same condition with excitation wavelength of 420 nm.

2.5. Photoelectrochemical measurement

Five milligrams of photocatalysts and 10 μL of Nafion solution (5 wt %) were dispersed in 1 mL of ethanol and then ultrasonically dispersed to prepare a homogeneous catalyst ink. Next, 40 μ L of the catalyst ink was deposited onto an area of 0.196 cm^2 on ITO conductive glass and then was dried in air. Photoelectrochemical characterization was performed in the three-electrode cell. CdS and L-CdS film, Ag/AgCl in saturated KCl solution, and Pt foil were used as working electrode, the reference electrode, and the counter electrode, respectively. The electrolyte was the aqueous solution of 0.1 mol/L of Na_2S and 0.1 mol/L of Na_2SO_3. The photocurrent was observed for each switch-on/-off ; event by using AM 1.5 G simulated sunlight plus filter with cutoff wavelength of 420 nm, and the applied potential of working electrode against the counter electrode was set to 0 V. Electrochemical impedance spectroscopy was carried out by CHI-760E potentiostat (Shanghai Chenhua). The amplitude of the alternating voltage is 10 mV, and the frequency range is from 1 Hz to 100 kHz.

3. Results and discussion

The atomic surface structure of CdS after laser irradiation treatment was directly characterized by aberration-corrected STEM analyses. The particle morphology of CdS was confirmed by SEM (Fig. 1a, b). Fig. 1c shows the atomic-resolution ABF images of L-CdS with laser irradiation treatment viewed from the [100] crystallographic direction. The continuous atomic arrangement matches well with the CdS lattices viewed from the [100] direction, as shown in the inset of Fig. 1. The d spacing of 0.326 nm in region 2 is corresponded to the (002) plane of CdS with hexagonal crystal structure [53,54]. Furtherly, the atomic positions of Cd and S atoms were clearly distinguished in the Fig. 1e (Zone 2), in which the dark atoms are assigned to Cd atoms surrounded by slightly bright S atoms. Fig. 1d shows the enlarged region (Zone 1) on the surface of CdS. Only dark Cd atoms within the thin shell of ~ 1 nm were observed with reduced brightness around Cd atoms, during which the structures are consistent with the simulation of the blue Cd atoms with the hexagonal crystal structure. The formation of metallic Cd clusters on CdS surface may be caused by the localized thermal eff ;ect of the pulsed laser, which rapidly breaks Cd-S bonds on CdS to subsequently reduce Cd^{2+} into metallic state Cd. The measured d spacing distance is slightly different with that in the literature [55]. It is possible that the surface Cd is slightly distorted due to that the stress is not completely released. The above results indicate that the metallic Cd clusters on CdS surface are *in-situ* formed after laser irradiation treatment.

In addition to electron microscopy, various spectral analyses were conducted for characterizing the samples. The XRD patterns of CdS and L-CdS are shown in Fig. 2a. The identified peaks of XRD patterns could be perfectly indexed to CdS with hexagonal structure (ICDD-PDF No. 41-1049). No new diffraction peak appears in the spectrum after laser irradiation treatment of CdS, probably due to the low Cd content. To

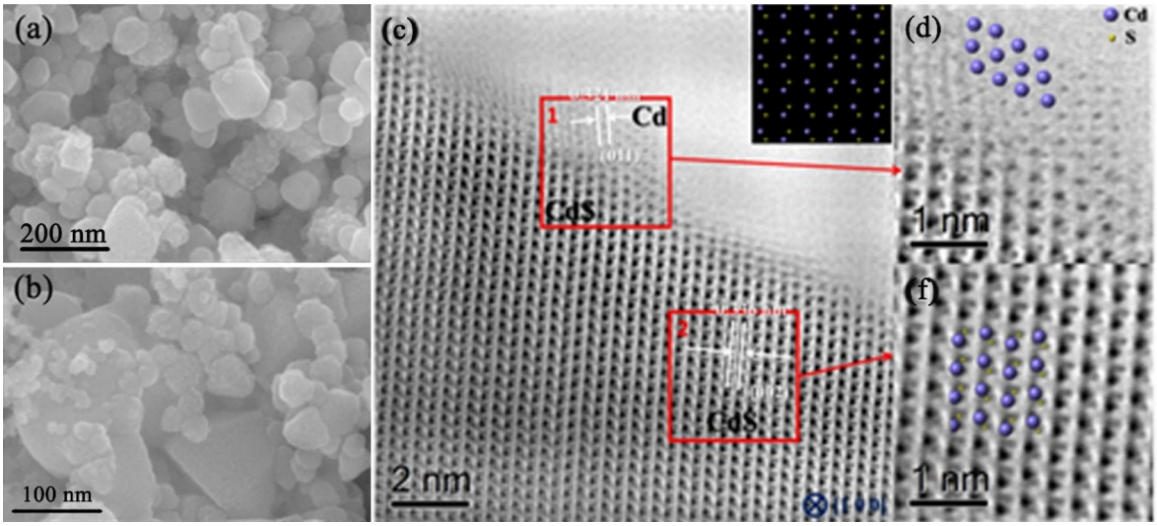

Fig. 1. (a, b) SEM images of CdS. (c) The atomic-resolution ABF STEM images of CdS with laser irradiation treatment viewed from the [100] crystallographic direction. The inset in Fig. 1c illustrates the crystal structure of CdS viewed from the [100] direction, where the larger blue spheres represent Cd atoms and the smaller yellow spheres represent S atoms. The d spacing of 0.321 nm in region 1 and The d spacing of 0.326 nm in region 2 correspond to the spacing of the (011) face of Cd and the (002) face of CdS, respectively. (d–f) The enlarged views of Fig. 1c in region 1 and 2 (For interpretation of the references to colour in this figure legend, the reader is referred to the web version of this article).

characterize the surface chemical states of L-CdS, the XPS spectra of the sample were measured. As shown in Fig. 2b, the peaks of Cd and S elements were observed. Fig. 2c shows the 3d electron spectrum of Cd, and the peaks located at 405.20 eV and 411.94 eV are corresponded to Cd $3d_{5/2}$ and Cd $3d_{3/2}$, respectively, indicating that the Cd^{2+} state of CdS. Compared with the pure CdS, the peaks of L-CdS shift toward lower binding energy, confirming the presence of metallic state Cd atoms from the reduction of Cd^{2+} by the laser irradiation treatment. As shown in Fig. 2d, the 2p electron spectrum of S can be fitted with two diffraction peaks located at 161.48 eV corresponding to S 2p3/2 and S 2p1/2 of S^{2-} in pure CdS, respectively. The atomic ratio of S on the surface of CdS and L-CdS is 31.48% and 28.96%, respectively, revealing that the localized thermal eff ;ect of the pulsed laser cause the evaporation loss of S atoms on the surface. Compared with the pure CdS, the peaks of S 2p in the L-CdS shift to higher energy, probably due to the loss of the S atoms on the surface and the build-in field formed in the energy alignment of Schottky junction.

To evaluate photocatalytic activity of CdS and L-CdS, the photocatalytic hydrogen evolution from water splitting under visible light excitation (> 420 nm) were conducted. It should be emphasized that no

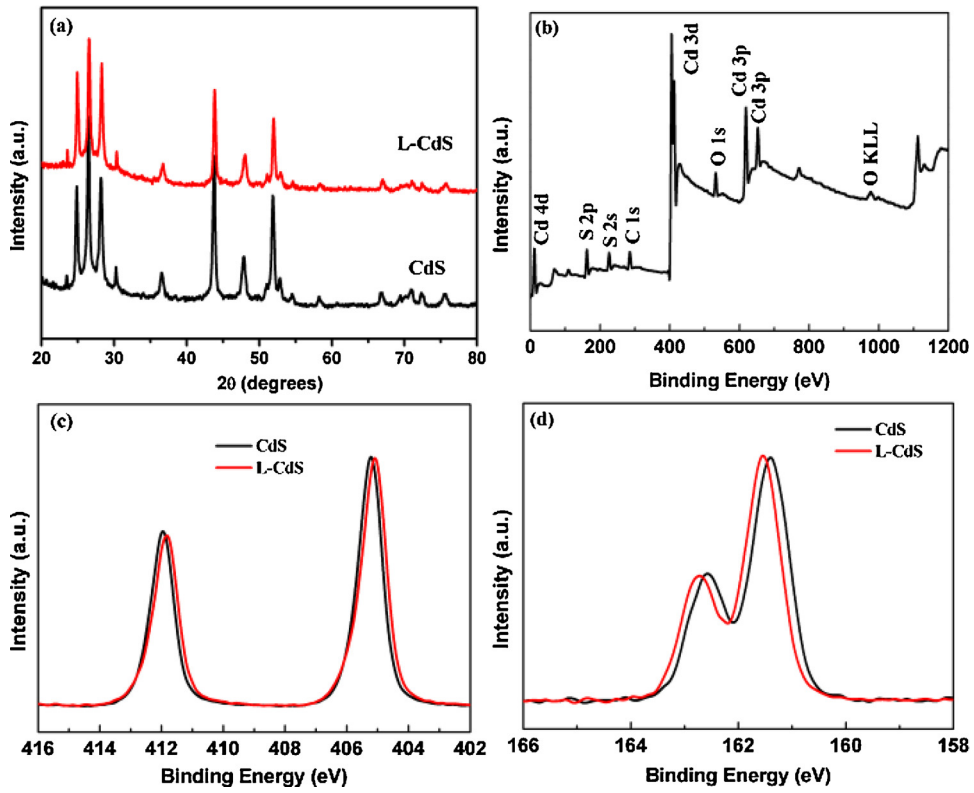

Fig. 2. (a) The XRD spectra of CdS and L-CdS. (b–d) The XPS spectra of L-CdS: (b) survey, (c) Cd 3d, and (d) S 2p.

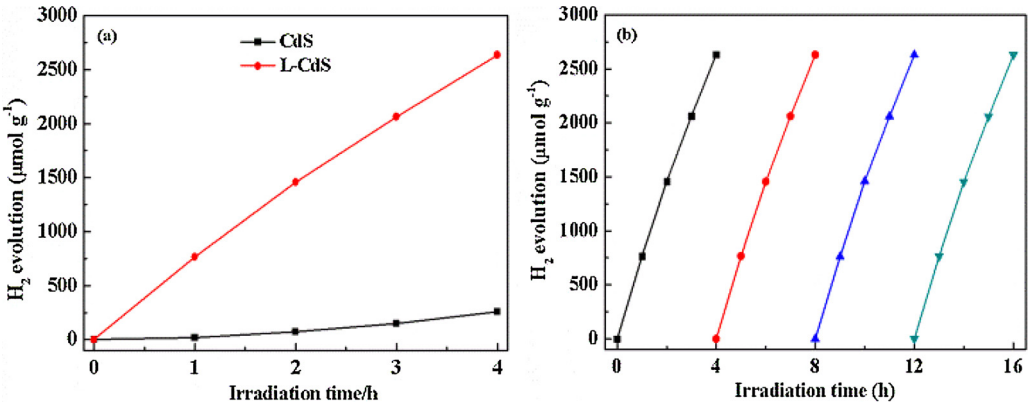

Fig. 3. (a) H_2 evolution of CdS and L-CdS (20 mg) in 100 mL deionized water with 0.1 M Na_2S and 0.1 M Na_2SO_3 under visible light irradiation (> 420 nm). (b) Cycling measurements of hydrogen evolution for L-CdS under visible light.

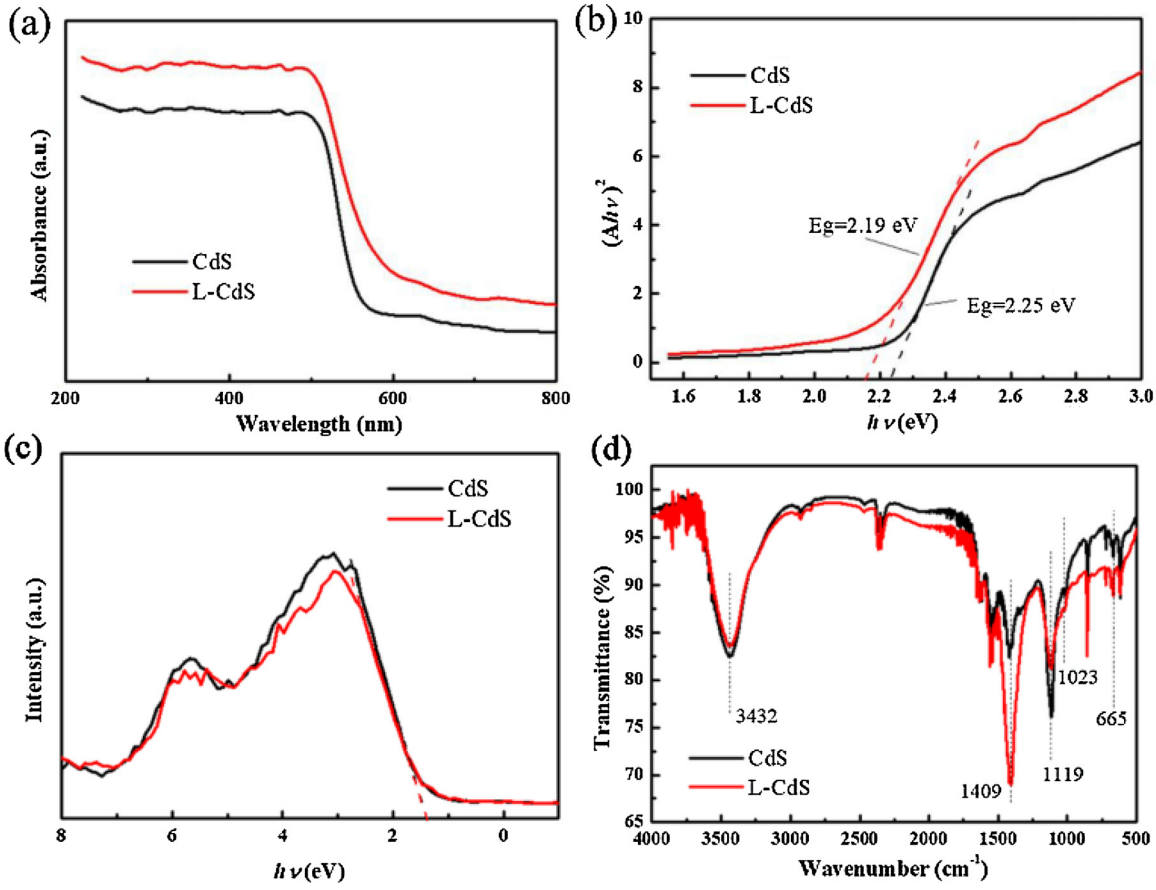

Fig. 4. (a) UV–vis absorptions spectra of CdS and L-CdS. (b) Tauc plots calculated from of (a), showing the bandgap of CdS in CdS and L-CdS. (c) Valance-band XPS spectra and (d) FTIR spectra of CdS and L-CdS.

Fig. 5. Photograph of CdS before and after laser treatment.

noble-metal co-catalysts such as Pt and Au and RuO_2 were added in the photocatalytic system. As shown in Fig. 3a, the total amount of hydrogen evolution over pure CdS is about 19.1 μmol g^{-1} under first hour of visible light irradiation. L-CdS shows 765.5 μmol g^{-1} of hydrogen evolution under the same test condition. And, the rate of hydrogen evolution over L-CdS in first hour is 40-time than that of pure CdS. It is revealed that the pulsed laser irradiation treatment of CdS can contribute to the enhancement of hydrogen evolution, probably owing to the *in-situ* formation of metallic Cd clusters on CdS surface. Fig. 3b shows the recycle runs of hydrogen evolution of L-CdS. After four runs, the hydrogen evolution rate has no obvious decrease, indicating the excellent stability of L-CdS under visible light irradiation. In addition,

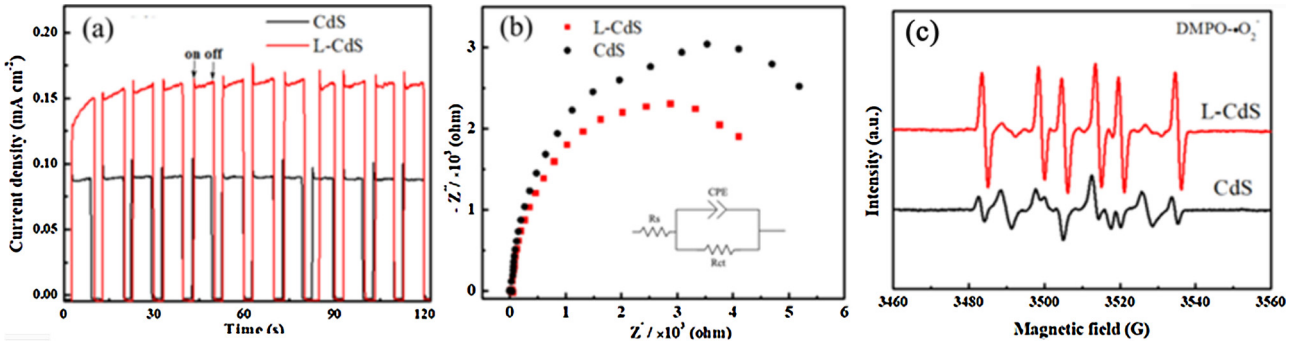

Fig. 6. a) Photocurrent responses, (b) electrochemical impedance, and EPR spectra of (c) DMPO-$^{\cdot}O^{2-}$ in methanol suspension of CdS and L-CdS.

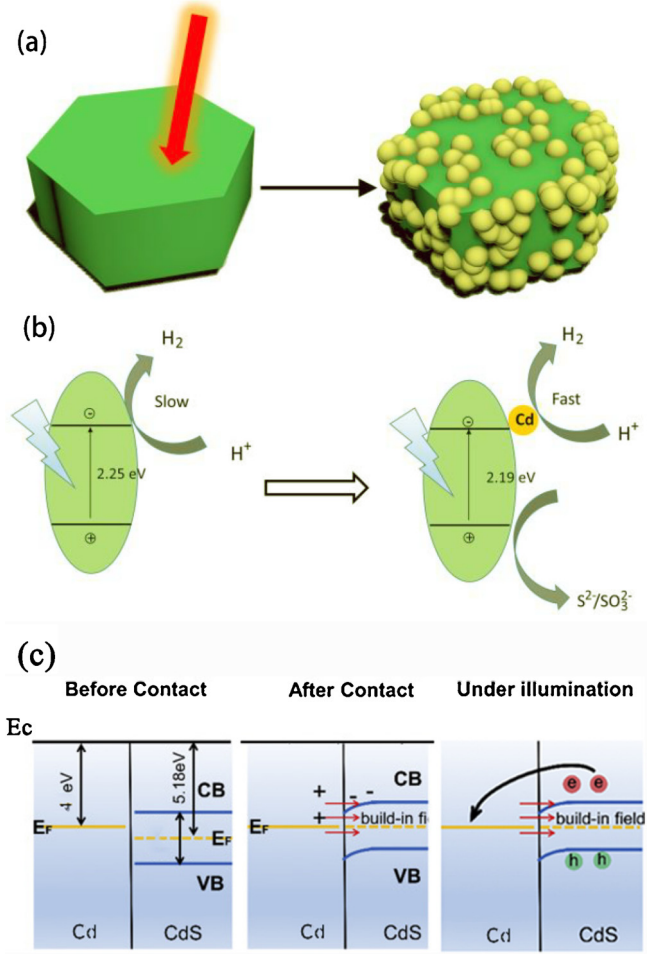

Fig. 7. (a) A schematic of the laser irradiation induced form CdS/Cd Schottky junction, (b) the schematic diagram of the mechanisms for the improved photocatalytic hydrogen evolution performance, and (c) band structure illustration of the carrier transfer process of CdS/Cd Schottky junction.

the QE of L-CdS is 0.82% under the excitation wavelength of 420 nm.

In order to explore the mechanism of the enhancement of hydrogen evolution, several analyses were conducted. The photocatalytic efficiency is usually determined by the balance of thermody-namics and kinetics of light-harvesting processes, charge transport and separation processes, and catalytic reaction. Fig. 4a shows the UV–vis spectra of CdS and L-CdS. Compared with the pure CdS, the absorption edge of CdS in L-CdS obviously shows a red-shift, and the intensity of the light absorption in the full spectrum range is also significantly enhanced, revealing that more charge carriers could be generated for the enhancement of hydrogen evolution under visible light irradiation. Fig. 5 shows the photograph of the sample before and after laser treatment. After laser treatment, the sample color is deepened, which is consistent with the results of UV–vis absorptions spectra. In addition, the direct band gap of the samples can be obtained by fitting the linear portion of the Tauc curves $((Ah\upsilon)^2$ vs $h\upsilon)$ (Fig. 4b) [56]. The band gap value of pure CdS is calculated to be 2.25 eV, which is in agreement with the literature value (2.25 eV) [22]. While the band gap value of CdS after laser treatment narrows to be 2.19 eV, probably because the evaporation loss of S atoms on the surface, and then destroys the original state of CdS surface to increase the opportunity of the formation of dangling bond on CdS surface, which may cause the narrow of the bandgap of CdS. The enhanced visible light absorption may be derived from the electronic interaction between the Cd and CdS at the interface. In order to characterize the valence band of CdS and L-CdS, valence-band XPS spectra were obtained. As shown in Fig. 4c, the valence band maximum is 1.6 eV for both samples, which is consistent with that in the literature [56].

The FT-IR measurement of CdS and L-CdS after photocatalytic test was conducted. As shown in Fig. 4d, the absorption peaks at 1119, 1023, and 665 cm^{-1} are assigned to the vibration of Cd-S bonds [57,58]. In addition, the broad band around 3432 cm^{-1} is corresponded to the stretch and bending vibration of $-OH$ or H_2O.[22] The peak at 1409 cm^{-1} results from the adsorbed S^{2-} and SO_3^{2-} ions, which could quickly capture photogenerated holes to enhance hydrogen evolution activity on CdS surface [59]. It is clearly observed that the adsorption of S^{2-} and SO_3^{2-} ions over L-CdS is enhanced compared to pure CdS. So L-CdS shows stronger adsorption capacity of the sacrificial agents such as S^{2-} and SO_3^{2-} to promote the consumption of photogenerated holes, enhancing the separation of electron-hole pairs and thus the hydrogen evolution activity of L-CdS.

To further characterize the separation and transportation of photogenerated electron-hole pairs, the photocurrent density and electrochemical impedance were measured. Fig. 6a shows the reproducible photocurrent responses for each switch-off and switch-on light cycles for CdS and L-CdS electrodes under visible light excitation (> 420 nm). The photocurrent density of L-CdS is almost 2-times than that of pure CdS, indicating the higher separation efficiency of photogenerated electron-hole pairs in L-CdS, because the metallic Cd clusters on surface of CdS can accept photogenerated electrons from CdS through the formation of Schottky junction between Cd clusters and CdS. In addition, L-CdS shows a smaller arc radius than CdS in the electrochemical impedance Nyquist plots (Fig. 6b), indicating that a smaller charge transfer resistance (Rct) results in the higher carrier separation efficiency of L-CdS. As shown in Fig. 6c, the stronger DMPO-$\bullet O_2^-$ signal can be observed over L-CdS than that of CdS, indicating the accumulation of photogenerated electrons in L-CdS. Thus, the formation of CdS/Cd Schottky junction can accelerate the separation and transfer of photogenerated electron-hole pairs in L-CdS to surface for photocatalytic hydrogen production.

As shown in Fig. 7, the pulsed laser irradiation induces the in-situ formation of metallic Cd clusters on CdS surface to construct the

Table 1
Comparison of photocatalytic H_2-produ results.

photocatalyst	Improved times[a] (compared with pure CdS)	Sacrifice reagent	References
CdS Nanoparticle/Cd Nanosheets	4.6	Na_2S/Na_2SO_3	[48]
Cd/CdS	7.5	Na_2S/Na_2SO_3	[62]
FeSe/CdS	7	Na_2S/Na_2SO_3	[63]
Ni3C/CdS	7.76	Na_2S/Na_2SO_3	[64]
Au/CdS	2.3	Na_2S/Na_2SO_3	[65]
MoS_2/CdS	6.6	lactic acid	[66]
Cd/CdS	40	Na_2S/Na_2SO_3	This work

[a] Improving times = H_2-production rate of the optimal catalyst/H_2-production rate of CdS.

Schottky junction between Cd clusters and CdS. The mechanisms for the improved photocatalytic hydrogen evolution performance are illustrated in Fig. 7b. Firstly, the pulsed laser irradiation causes the band gap narrow of CdS, resulting in the enhancement of visible light absorption and the excitation of more electron–hole pairs. Secondly, the metallic Cd clusters on the CdS surface could capture the photogenerated electrons to improve the separation efficiency of electron-hole pairs, thus participating in the hydrogen production reaction. Finally, CdS/Cd has a stronger adsorption capacity of the sacrificial agents such as S^{2-} and SO_3^{2-} to promote the consumption of photogenerated holes and also enhance the separation of the photogenerated electron-hole pairs. Fig. 7c also shows the band structure illustration of the charge transfer process of CdS/Cd Schottky junction. The work function of CdS and metallic Cd clusters are 5.18 eV [60] and 4.08 eV [61] respectively. After contact, electrons in Cd will transfer to CdS until the Fermi level of the two materials are aligned, because the Fermi level of CdS is lower than that of metallic Cd. When CdS is excited by light irradiation, the photo-generated electrons on the surface of CdS will be driven by the build-in field and transferred to the surface of Cd. Therefore, all above factors favorably lead to the remarkably enhanced photocatalytic activity of visible light-driven hydrogen evolution from water splitting. We also compare the photocatalytic H_2-production activity of L-CdS with other state-of-the-art CdS-based photocatalysts reported in the literatures, as shown in Table 1. It can be determined that the as-prepared L-CdS has higher activity that the prepared CdS by other methods without Pt as co-catalysts.

4. Conclusions

In summary, the CdS/Cd Schottky junction induced from the pulsed laser irradiation is successfully developed as photocatalyst for efficient visible light-driven hydrogen evolution from water splitting, owing to that the *in-situ* formation of metallic Cd clusters on CdS surface can accept excited electrons through the Schottky junction to efficiently accelerate the separation of electron-hole pairs and endow more electrons for photocatalytic reduction reaction. Moreover, CdS/Cd has a stronger adsorption capacity of the sacrificial agents such as S^{2-} and SO_3^{2-} to promote the consumption of photogenerated holes, and the bandgap narrow of CdS also benefits the stronger light absorption, thus contributing to hydrogen evolution. This work may provide a new approach to develop heterojunction-based photocatalysts for efficient solar-to-chemical conversion.

Declaration of Competing Interest

The authors declare that they have no known competing financial interests or personal relationships that could have appeared to influence the work reported in this paper.

Acknowledgments

This work was under the support from the National Natural Science Foundation of China (Grant No. 51802211, 51572183, and 21673001). I am very grateful to Professor Xiaolong Chen from the Institute of Physics of the Chinese Academy of Sciences for their guidance.

References

[1] N.S. Lewis, Toward cost-effective solar energy use, Science 315 (2007) 798.
[2] Y.X. Chen, K.N. Yang, B. Jiang, J.X. Li, M.Q. Zeng, L. Fu, Emerging two-dimensional nanomaterials for electrochemical hydrogen evolution, J. Mater. Chem. A 5 (2017) 8187–8208.
[3] Z. Wang, C. Li, K. Domen, Recent developments in heterogeneous photocatalysts for solar-driven overall water splitting, Chem. Soc. Rev. 48 (2019) 2109–2125.
[4] M. Grätzel, Photoelectrochemical cells, Nature 414 (2001) 338.
[5] B.A. Pinaud, J.D. Benck, L.C. Seitz, A.J. Forman, Z. Chen, T.G. Deutsch, B.D. James, K.N. Baum, G.N. Baum, S. Ardo, H. Wang, E. Miller, T.F. Jaramillo, Technical and economic feasibility of centralized facilities for solar hydrogen production via photocatalysis and photoelectrochemistry, Energy Environ. Sci. 6 (2013) 1983–2002.
[6] Y. Goto, T. Hisatomi, Q. Wang, T. Higashi, K. Ishikiriyama, T. Maeda, Y. Sakata, S. Okunaka, H. Tokudome, M. Katayama, S. Akiyama, H. Nishiyama, Y. Inoue, T. Takewaki, T. Setoyama, T. Minegishi, T. Takata, T. Yamada, K. Domen, A Particulate photocatalyst water-splitting panel for large-scale solar hydrogen generation, Joule 2 (2018) 509–520.
[7] J. Huang, J. Han, R. Wang, Y. Zhang, X. Wang, X. Zhang, Z. Zhang, Y. Zhang, B. Song, S. Jin, Improving electrocatalysts for oxygen evolution using $NixFe_{3-x}O_4$/Ni hybrid nanostructures formed by solvothermal synthesis, ACS Energy Lett. 3 (2018) 1698–1707.
[8] Q. Fu, T. Wu, G. Fu, T. Gao, J. Han, T. Yao, Y. Zhang, W. Zhong, X. Wang, B. Song, Skutterudite-type ternary $Co_{1-x}Ni_xP_3$ nanoneedle array electrocatalysts for enhanced hydrogen and oxygen evolution, ACS Energy Lett. 3 (2018) 1744–1752.
[9] A. Fujishima, K. Honda, Electrochemical photolysis of water at a semiconductor electrode, Nature 238 (1972) 37–38.
[10] K. Sayama, H. Arakawa, Photocatalytic decomposition of water and photocatalytic reduction of carbon dioxide over zirconia catalyst, J. Phys. Chem. 97 (1993) 531–533.
[11] A. Kudo, H. Kato, S. Nakagawa, Water splitting into H_2 and O_2 on new $Sr_2M_2O_7$(M = Nb and Ta) photocatalysts with layered perovskite structures: factors affecting the photocatalytic activity, J. Phys. Chem. B 104 (2000) 571–575.
[12] S. Chen, T. Takata, K. Domen, Particulate photocatalysts for overall water splitting, Nat. Rev. Mater. 2 (2017) 17050.
[13] J. Sato, N. Saito, H. Nishiyama, Y. Inoue, New photocatalyst group for water decomposition of RuO_2-loaded p-block metal (In, Sn, and Sb) oxides with d^{10} configuration, J. Phys. Chem. B 105 (2001) 6061–6063.
[14] K. Ikarashi, J. Sato, H. Kobayashi, N. Saito, H. Nishiyama, Y. Inoue, Photocatalysis for water decomposition by RuO_2-dispersed $ZnGa_2O_4$ with d^{10} configuration, J. Phys. Chem. B 106 (2002) 9048–9053.
[15] T. Yanagida, Y. Sakata, H. Imamura, Photocatalytic decomposition of H_2O into H_2 and O_2 over Ga_2O_3 loaded with NiO, Chem. Lett. 33 (2004) 726–727.
[16] Y. Inoue, Photocatalytic water splitting by RuO2-loaded metal oxides and nitrides with d^0- and d^{10} -related electronic configurations, Energy Environ. Sci. 2 (2009) 364–386.
[17] W.N. Shi, X.W. Guo, C.X. Cui, K. Jiang, Z.J. Li, L.B. Qu, J.C. Wang, Controllable synthesis of Cu_2O decorated WO_3 nanosheets with dominant (001) facets for photocatalytic CO_2 reduction under visible -light irradiation, Appl. Catal. B-environ 243 (2019) 236–242.
[18] Z.R. Liu, X.Y. Liu, X.X. Gu, R.Q. Guo, W.W. Zhong, $Cu_{2-x}Se$ modification onto monoclinic $BiVO_4$ for enhanced photocatalytic activity under visible light, Nanoscale Res. Lett. 14 (2019).
[19] A. Kudo, Y. Miseki, Heterogeneous photocatalyst materials for water splitting, Chem. Soc. Rev. 38 (2009) 253–278.
[20] T. Di, Q. Xu, W. Ho, H. Tang, Q. Xiang, J. Yu, Review on metal sulphide-based Z-scheme photocatalysts, ChemCatChem 11 (2019) 1394–1411.
[21] J. Fu, Q. Xu, J. Low, C. Jiang, J. Yu, Ultrathin 2D/2D WO_3/g-C_3N_4 step-scheme H_2 production photocatalyst, Appl. Catal. B 243 (2019) 556–565.
[22] J. Low, B. Dai, T. Tong, C. Jiang, J. Yu, In situ irradiated X-ray photoelectron spectroscopy investigation on a direct Z-scheme TiO_2/CdS composite film photocatalyst, Adv. Mater. 31 (2019) 1802981.
[23] S. Wang, B. Zhu, M. Liu, L. Zhang, J. Yu, M. Zhou, Direct Z-scheme ZnO/CdS hierarchical photocatalyst for enhanced photocatalytic H_2 production activity,

Appl. Catal. B 243 (2019) 19–26.
[24] R. Sasikala, A.R. Shirole, V. Sudarsan, K.G. Girija, R. Rao, C. Sudakar, S.R. Bharadwaj, Improved photocatalytic activity of indium doped cadmium sulfide dispersed on zirconia, J. Mater. Chem. 21 (2011) 16566–16573.
[25] Y.P. Liu, S.J. Shen, J.T. Zhang, W.W. Zhong, X.H. Huang, $Cu_{2-x}Se$/CdS composite photocatalyst with enhanced visible light photocatalysis activity, Appl. Surf. Sci. 478 (2019) 762–769.
[26] Q. Li, B. Guo, J. Yu, J. Ran, B. Zhang, H. Yan, J.R. Gong, Highly Efficient visible-light-driven photocatalytic hydrogen production of CdS-cluster-decorated graphene nanosheets, J. Am. Chem. Soc. 133 (2011) 10878–10884.
[27] Q. Xiang, B. Cheng, J. Yu, Hierarchical porous CdS nanosheet-assembled flowers with enhanced visible-light photocatalytic H_2 production performance, Appl. Catal. B 138–139 (2013) 299–303.
[28] J. Jin, J.G. Yu, G. Liu, P.K. Wong, Single crystal CdS nanowires with high visible-light photocatalytic H_2 production performance, J. Mater. Chem. A 1 (2013) 10927–10934.
[29] J. Yu, Y. Yu, P. Zhou, W. Xiao, B. Cheng, Morphology-dependent photocatalytic H_2 production activity of CdS, Appl. Catal. B-environ 156–157 (2014) 184–191.
[30] J. Zhang, S. Wageh, A. Al-Ghamdi, J. Yu, New understanding on the different photocatalytic activity of wurtzite and zinc-blende CdS, Appl. Catal. B 192 (2016) 101–107.
[31] Z. Chen, C. Feng, W. Li, Z. Sun, J. Hou, X. Li, L. Xu, M. Sun, Y. Bu, Enhanced visible-light-driven photocatalytic activities of 0D/1D heterojunction carbon quantum dot modified CdS nanowires, Chin. J. Catal. 39 (2018) 841–848.
[32] H. Zhai, X. Liu, P. Wang, B. Huang, Q. Zhang, Enhanced photocatalytic H_2 production of $Mn_{0.5}Cd_{0.5}S$ solid solution through loading transition metal sulfides XS (X = Mo, Cu, Pd) cocatalysts, Appl. Surf. Sci. 430 (2018) 515–522.
[33] Y. Zhang, Z. Jin, H. Yuan, G. Wang, B. Ma, Well-regulated nickel nanoparticles functional modified ZIF-67 (Co) derived Co_3O_4/CdS p-n heterojunction for efficient photocatalytic hydrogen evolution, Appl. Surf. Sci. 462 (2018) 213–225.
[34] Y. Zhao, Z.-B. Fang, W. Feng, K. Wang, X. Huang, P. Liu, Hydrogen production from pure water via piezoelectric-assisted visible-light photocatalysis of CdS nanorod arrays, ChemCatChem 10 (2018) 3397–3401.
[35] T. Di, B. Cheng, W. Ho, J. Yu, H. Tang, Hierarchically CdS–Ag_2S nanocomposites for efficient photocatalytic H_2 production, Appl. Surf. Sci. 470 (2019) 196–204.
[36] T. Di, B. Zhu, J. Zhang, B. Cheng, J. Yu, Enhanced photocatalytic H_2 production on CdS nanorod using cobalt-phosphate as oxidation cocatalyst, Appl. Surf. Sci. 389 (2016) 775–782.
[37] Y. Wang, Y. Wang, R. Xu, Photochemical deposition of Pt on CdS for H_2 evolution from water: markedly enhanced activity by controlling Pt reduction environment, J. Phys. Chem. C 117 (2013) 783–790.
[38] S. Cao, C.-J. Wang, X.-J. Lv, Y. Chen, W.-F. Fu, A highly efficient photocatalytic H_2 evolution system using colloidal CdS nanorods and nickel nanoparticles in water under visible light irradiation, Appl. Catal. B-environ 162 (2015) 381–391.
[39] X. Chen, W. Chen, P. Lin, Y. Yang, H. Gao, J. Yuan, W. Shangguan, In situ photo-deposition of nickel oxides on CdS for highly efficient hydrogen production via visible-light-driven photocatalysis, Catal. Commun. 36 (2013) 104–108.
[40] S. Cao, Y. Chen, C.J. Wang, P. He, W.F. Fu, Highly efficient photocatalytic hydrogen evolution by nickel phosphide nanoparticles from aqueous solution, Chem. Commun. 50 (2014) 10427–10429.
[41] S. Ma, X. Xu, J. Xie, X. Li, Improved visible-light photocatalytic H_2 generation over CdS nanosheets decorated by NiS_2 and metallic carbon black as dual earth-abundant cocatalysts, Chin. J. Catal. 38 (2017) 1970–1980.
[42] L.J. Zhang, R. Zheng, S. Li, B.K. Liu, D.J. Wang, L.L. Wang, T.F. Xie, Enhanced photocatalytic H_2 generation on cadmium sulfide nanorods with cobalt hydroxide as cocatalyst and insights into their photogenerated charge transfer properties, ACS Appl. Mater. Interfaces 6 (2014) 13406–13412.
[43] Y. Liu, S. Ding, Y. Shi, X. Liu, Z. Wu, Q. Jiang, T. Zhou, N. Liu, J. Hu, Construction of CdS/CoO_x core-shell nanorods for efficient photocatalytic H_2 evolution, Appl. Catal. B-Environ. 234 (2018) 109–116.
[44] B. Chai, M. Xu, J. Yan, Z. Ren, Remarkably enhanced photocatalytic hydrogen evolution over MoS_2 nanosheets loaded on uniform CdS nanospheres, Appl. Surf. Sci. 430 (2018) 523–530.
[45] B. Ma, R. Zhang, K. Lin, H. Liu, X. Wang, W. Liu, H. Zhan, Large-scale synthesis of noble-metal-free phosphide/CdS composite photocatalysts for enhanced H_2 evolution under visible light irradiation, Chin. J. Catal. 39 (2018) 527–533.
[46] Q. Li, T. Shi, X. Li, K. Lv, M. Li, F. Liu, H. Li, M. Lei, Remarkable positive effect of Cd$(OH)_2$ on CdS semiconductor for visible-light photocatalytic H_2 production, Appl. Catal. B-Environ. 229 (2018) 8–14.
[47] B. Wang, S. He, W. Feng, L. Zhang, X. Huang, K. Wang, S. Zhang, P. Liu, Rational design and facile in situ coupling non-noble metal Cd nanoparticles and CdS nanorods for efficient visible-light-driven photocatalytic H_2 evolution, Appl. Catal. B-Environ. 236 (2018) 233–239.
[48] L. Shang, B. Tong, H. Yu, G.I.N. Waterhouse, C. Zhou, Y. Zhao, M. Tahir, L.-Z. Wu, C.-H. Tung, T. Zhang, CdS Nanoparticle-decorated Cd Nanosheets for efficient visible light-driven photocatalytic hydrogen evolution, Adv. Energy Mater. 6 (2016) 1501241.
[49] Q. Li, X. Li, S. Wageh, A.A. Al-Ghamdi, J.G. Yu, CdS/Graphene nanocomposite photocatalysts, Adv. Energy Mater. 5 (2015) 1500010.
[50] A. Singh, A.S.K. Sinha, Active CdS/rGO photocatalyst by a high temperature gas-solid reaction for hydrogen production by splitting of water, Appl. Surf. Sci. 430 (2018) 184–197.
[51] Z. Zhu, Y. Han, C. Chen, Z. Ding, J. Long, Y. Hou, Reduced graphene oxide-cadmium sulfide nanorods decorated with silver nanoparticles for efficient photocatalytic reduction carbon dioxide under visible light, ChemCatChem 10 (2018) 1627–1634.
[52] W. Zhong, Z. Lin, S. Feng, D. Wang, S. Shen, Q. Zhang, L. Gu, Z. Wang, B. Fang, Improved oxygen evolution activity of IrO_2 by in situ engineering of an ultra-small Ir sphere shell utilizing a pulsed laser, Nanoscale 11 (2019) 4407–4413.
[53] J. Li, Y. Peng, X. Qian, J. Lin, Few-layer Co-doped MoS_2 nanosheets with rich active sites as an efficient cocatalyst for photocatalytic H_2 production over CdS, Appl. Surf. Sci. 452 (2018) 437–442.
[54] Z. Zhu, Y. Han, C. Chen, Z. Ding, J. Long, Y. Hou, Reduced graphene oxide-cadmium sulfide nanorods decorated with silver nanoparticles for efficient photocatalytic reduction carbon dioxide under visible light, ChemCatChem 10 (2018) 1627–1634.
[55] E. Rossmanith, X-ray measurement of the root-mean-square displacement of the atoms in cadmium single crystals, Acta Crystallogr. A 34 (1978) 497–500.
[56] G.S. Shahane, B.M. More, C.B. Rotti, L.P. Deshmukh, Studies on chemically deposited $CdS_{1-x}Se_x$ mixed thin films, Mater. Chem. Phys. 47 (1997) 263–267.
[57] H.G. Yu, W. Zhong, X. Huang, P. Wang, J.G. Yu, Suspensible cubic-phase CdS nanocrystal photocatalyst: facile synthesis and highly efficient H_2 evolution performance in a sulfur-rich system, ACS Sustain. Chem. Eng. 6 (2018) 5513–5523.
[58] S.-H. Yu, L. Shu, J. Yang, K.-B. Tang, Y. Xie, Y.-T. Qian, Y.-H. Zhang, Benzene-thermal synthesis and optical properties of CdS nanocrystalline, Nanostruct. Mater. 10 (1998) 1307–1316.
[59] F. Vaquero, R.M. Navarro, J.L.G. Fierro, Influence of the solvent on the structure, morphology and performance for H_2 evolution of CdS photocatalysts prepared by solvothermal method, Appl. Catal. B-Environ. 203 (2017) 753–767.
[60] Y. Xu, M.A.A. Schoonen, Am. Min. 85 (2000) 543–556.
[61] D.R. Lide, CRC Handbook of Chemistry and Physics, (2008), pp. 12–114.
[62] Q.Z. Wang, J.J. Li, Y. Bai, J.H. Lian, H.H. Huang, Z.M. Li, Z.Q. Lei, W.F. Shangguan, Green Chem. 16 (2014) 2728–2735.
[63] W. Zhong, W. Tu, S. Feng, A. Xu, J. Alloys. Compd. 772 (2019) 669–674.
[64] S. Ma, Y. Deng, J. Xie, K. He, W. Liu, X. Chen, X. Li, Appl. Catal. B 227 (2018) 218–228.
[65] P. Wang, Y. Sheng, F. Wang, H. Yu, Appl. Catal. B 220 (2018) 561–569.
[66] X.H. Zhang, N. Li, J. Wu, Y.Z. Zheng, X. Tao, Appl. Catal. B 229 (2018) 227–236.